

PAPER • OPEN ACCESS

Design and test of a setup for calorimetric measurements of AC transport losses in HTS racetrack coils



To cite this article: Carlos Roberto Vargas-Llanos *et al* 2023 *Supercond. Sci. Technol.* **36** 045015

View the [article online](#) for updates and enhancements.

You may also like

- [Temperature dependence of critical currents and ac transport losses in \$\(\text{Bi,Pb}\)_2\text{Sr}_2\text{Ca}_2\text{Cu}_3\text{O}_x\$ and \$\text{YBa}_2\text{Cu}_3\text{O}_y\$ tapes](#)
Guo Min Zhang, D C Knoll, D N Nguyen et al.
- [Power dissipation in HTS coated conductor coils under the simultaneous action of AC and DC currents and fields](#)
Boyang Shen, Chao Li, Jianzhao Geng et al.
- [Calorimetric AC loss measurement of \$\text{MgB}_2\$ superconducting tape in an alternating transport current and direct magnetic field](#)
K W See, X Xu, J Horvat et al.

Design and test of a setup for calorimetric measurements of AC transport losses in HTS racetrack coils

Carlos Roberto Vargas-Llanos¹ , Joachim Krämer², Mathias Noe¹
and Francesco Grilli^{1,*} 

¹ Institute for Technical Physics (ITEP) of the Karlsruhe Institute of Technology (KIT), 76131 Karlsruhe, Germany

² Krämer Energietechnik GmbH & Co. KG, 34289 Zierenberg, Germany

E-mail: francesco.grilli@kit.edu

Received 17 October 2022, revised 9 February 2023

Accepted for publication 13 February 2023

Published 3 March 2023



Abstract

The estimation and measurement of AC losses in coils based on high-temperature superconductors (HTS) are relevant aspects of HTS applications. They influence the cooling power requirement, operating temperature and efficiency, which can be decisive in the construction and implementation of superconducting equipment, such as superconducting electrical machines. The measurement of losses due to AC transport current (without external magnetic field) is not an easy task. Several efforts have been made to measure these AC transport losses in superconducting coils with a calorimetric approach by trying to minimize the influence of the environment, improve the accuracy and ensure the reproducibility of the results. This work presents the design and construction of a setup to measure transport AC losses in high-temperature superconducting coils based on a calorimetric approach (boil-off method). The evaporated cryogen (nitrogen) related to the dissipation of energy is collected by using a 3D printed bubble collector that guides the gas into a flow sensor. A box-inside-a-box approach is used to surround the measurement chamber with a cryogenic environment. This approach allows re-directing the heat transfer from the surroundings into an intermediate zone (space between external and internal box). Since this intermediate zone operates under cryogenic temperatures, the noise and the heat transfer in the internal part of the setup are reduced. A statistical analysis of the results based on a standard load cycle, average value, and standard deviation calculations allows assessing the variability in the measurements and expressing the results as average value and uncertainty range. The calibration and reproducibility of the measurements are verified with a set of resistors under different conditions and during different weeks. Finally, the AC transport losses in a racetrack coil for an electrical machine application are measured and compared with 3D simulation results based on the homogenization of the T-A formulation.

* Author to whom any correspondence should be addressed.



Original Content from this work may be used under the terms of the [Creative Commons Attribution 4.0 licence](https://creativecommons.org/licenses/by/4.0/). Any further distribution of this work must maintain attribution to the author(s) and the title of the work, journal citation and DOI.

Keywords: high-temperature superconductors, AC losses, superconducting coil, calorimetric method, T-A formulation

(Some figures may appear in colour only in the online journal)

1. Introduction

The high current capacity and zero DC resistivity of high-temperature superconductors (HTS) has encouraged applications in several fields [1]. In fact, HTS electrical properties have inspired numerous research and development activities on electrical machines [2], energy storage [3], and fault current limiters [4]. In particular, the potential weight and size reduction related to HTS applications has motivated the development of new superconducting generators for wind turbine applications [5–9], where more compact and efficient machines are aimed within the current development of renewable energies. Most of these applications rely on the proper design, characterisation, and performance of superconducting coils.

Despite their zero DC resistance, HTS experience energy dissipation under time changing current or magnetic field [10]. These losses influence the cooling power requirement, operating temperature and efficiency, which can be decisive in the construction and wide implementation of superconducting devices. This work presents the design and test of a setup to measure AC transport losses in HTS coils.

There are two main methodologies commonly used to measure AC transport losses in HTS coils, the electric method and the calorimetric method [11, 12]. The electric method is based on the measurement of the current and the voltage in the coil. The voltage can be separated in two parts, a pure inductive component (90° shifted with respect to the current) and a 'resistive' (loss) component (in phase with the current) [13, 14]. The inductive component is usually larger than the loss component. Therefore, the efficiency of the method relies on cancelling the inductive component of the voltage to measure accurately the loss component. For this purpose, a compensation circuit (pick-up coil or variable transformer) and a lock-in amplifier are generally used. However, the inductive component of the voltage in HTS coils can be several orders of magnitude larger than the AC loss component [15, 16]. Therefore, it can be difficult to completely cancel the inductive component. Moreover, the measurement approach can be strongly influenced by the electromagnetic conditions of the environment (metallic and ferromagnetic parts, energized magnets, experiments, or cranes close to the setup) [11, 17]. For these reasons, the calorimetric method is adopted in this case. This approach does not require a compensation circuit, it is not strongly influenced by the electromagnetic conditions of the environment and is faster to implement [17–19].

In the implemented calorimetric approach, the evaporated cryogen (nitrogen) due to the AC losses in the coil is collected and its flow is measured. The flow of evaporated nitrogen is translated into dissipated power by using a previously measured calibration curve. This approach is known as the boil-off method and has been applied to measure the AC losses in

superconducting samples [20]; cables [21–23] and HTS coils under different operating conditions [19, 24–28]. In this work, a box-inside-a-box approach is used to surround the measurement chamber with a cryogenic environment. The approach allows re-directing the heat transfer from the surroundings into an intermediate zone. This space between the external and the internal box operates under cryogenic temperatures. Therefore, the heat transfer and the noise in the internal part of the setup are minimized. The measurement of the flow is post-processed through a statistical analysis based on a standard load cycle, average value, and standard deviation. This approach allows assessing the variability in the measurements and expressing the results as average value and uncertainty. Moreover, the reliability of the setup is studied by verifying the reproducibility of the results under different conditions in the calibration stage.

In this work, the losses due to AC transport current (without an external magnetic field) are measured in a HTS coil. The description of this coil is introduced first in section 2, which includes the main characteristics of the HTS tape, critical current and inductance measurement results. This section presents also an estimation of the transport losses in the coil based on the homogenization of the T-A formulation in 3D and a comparison with 2D simulation results. Then, the design of the AC transport losses measurement setup is introduced in section 3. Finally, section 4 presents the calibration of the setup and AC transport losses measurements results. All the findings of the work are summarized in the conclusions (section 5).

2. Coil description

This section presents the basic design and construction of the coil. The HTS tape is described first, and measurements of the critical current of the tape are presented. Then, the geometry and main parameters of the coil are discussed.

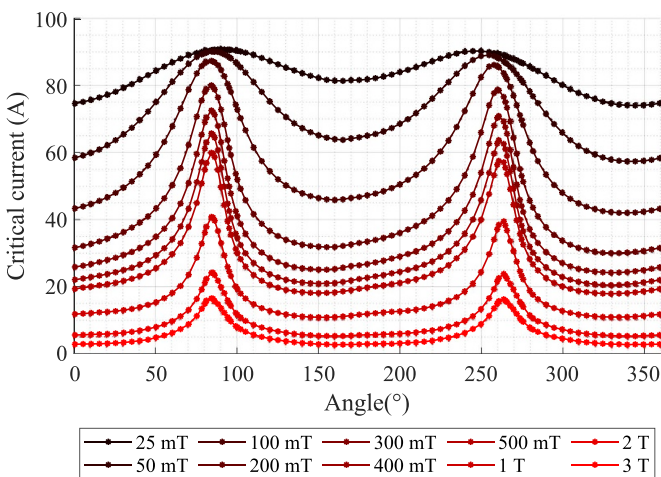
2.1. Tape description and characterisation

The tape used in the coil was manufactured by SuperOx, and the superconducting material is yttrium barium copper oxide (YBCO) [29]. The dimensions of the tape are 2 mm in width and 0.12 mm in thickness, with a copper stabilizer layer on both sides. The main characteristics are summarized in table 1, which also shows basic critical current measurements of the production batch and a brief description of the structure of the tape.

One of the most important parameters of the tape is the critical current (I_c) since it provides the maximum current capacity of the individual tape. Moreover, a proper characterisation of the I_c of the tape for different applied magnetic field amplitudes and directions is necessary to estimate the critical

Table 1. Main characteristics of the HTS tape.

Dimensions	Width	2 mm
	Thickness	0.12 mm
Structure	Copper stabilizer	20 μm per side
	Silver layer HTS side	2 μm
	Silver layer substrate side	1 μm
	Superconducting layer (YBCO)	2.5 μm
Electrical properties	Substrate (Hastelloy C-276)	40 μm
	Nominal I_c (77 K self-field)	60 A
	I_c measured by manufacturer (77.3 K self-field)	$I_{c-\text{min}} = 80$ A $I_{c-\text{avg}} = 83$ A $I_{c-\text{max}} = 88$ A
	Minimum bending radius	10 mm
Mechanical properties		

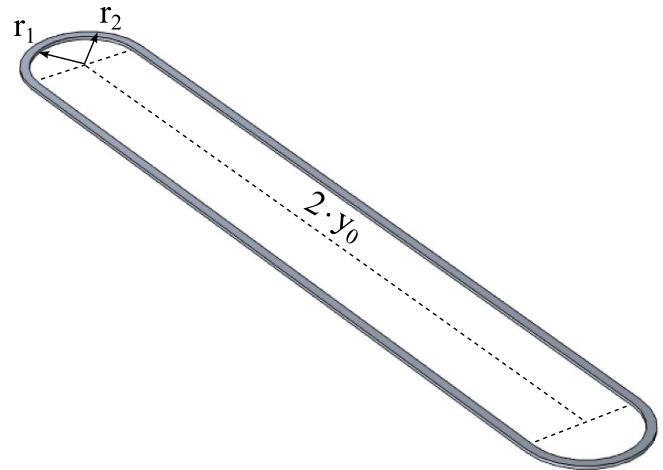
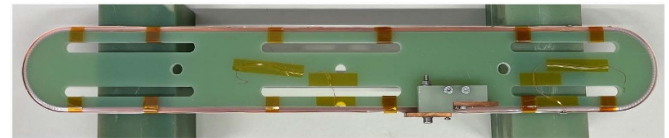
**Figure 1.** Measurements of the critical current of the HTS tape at 77 K as a function of magnetic field amplitude and direction. An angle of 0° represents a field perpendicular to the wide face of the tape; an angle of 90° represents a parallel one.

current of the coil, and to build models that allow studying the electromagnetic behaviour and estimate losses. For these reasons, measurements of the critical current of a sample of the tape were done with different magnetic field magnitudes and directions. Figure 1 shows the I_c measurement results at 77 K.

2.2. Coil geometry and characterisation

The coil is a scale-down version (1:3) of the stator coil of an electrical machine, it has a racetrack shape and represents one of the three types of coils necessary to build the star configuration introduced in [30]. The dimensions of the coil are presented in figure 2.

Figure 3 shows a picture of the constructed coil, which uses a total of 59.7 m of HTS tape. The former of the coil is made of glass fibre reinforced plastic to avoid possible induced currents that can increase the overall AC losses in the coil. Copper connectors are soldered to the tape to allow a standard connection with cables to energize the coil. The turn-to-turn insulation is PEN-foil 0.016 mm thick and 6 mm wide. The insulation is

**Figure 2.** Geometry and dimensions of the racetrack coil. The coil is made with 48 turns of HTS tape and has the following dimensions: $r_1 = 36$ mm, $r_2 = 42$ mm, and $2 \cdot y_0 = 500$ mm.**Figure 3.** Picture of the constructed coil that is used to measure AC transport losses.

co-wound with the HTS tape in the middle, and the coil is not impregnated.

The inductance of the coil is first estimated with a stationary 3D finite element model developed in Comsol Multiphysics. The inductance estimated with this simulation is 2.13 mH. These estimations are verified with measurements done with a LCR meter (Agilent U1733C—measurement frequency 1 kHz) in cold (covered by liquid nitrogen) and warm (ambient temperature) conditions. The measured inductance is $L_{\text{cold}} = 1.97$ mH ($L_{\text{warm}} = 2.01$ mH), which represents a deviation of 8.12% in cold conditions (5.97% in warm conditions), by considering the measurement results as the reference. The superconducting turns are fixed with an external Kapton tape (which can be seen in figure 3). Since there are no mechanical parts putting pressure to keep the superconducting turns in place and the compactness of the turns is not homogeneous along the coil, the thickness of the superconducting turns changes slightly along the length of the coil, which is one of the causes of discrepancies between inductance simulation and measurements. This effect is more meaningful when the coil is cooled down, since the glass-fiber reinforced plastic (GFRP) former shrinks with the decrease in temperature and gives more space for the HTS turns to relax and lose compactness.

The geometry of the coil has two straight and two circular parts. Therefore, it can not be directly reduced into a 2D arrangement for simulations without careful review. Moreover, the magnetic field tends to be higher in the inner part of the circular section [31], which can cause a higher current penetration in this zone. For these reasons, a 3D model

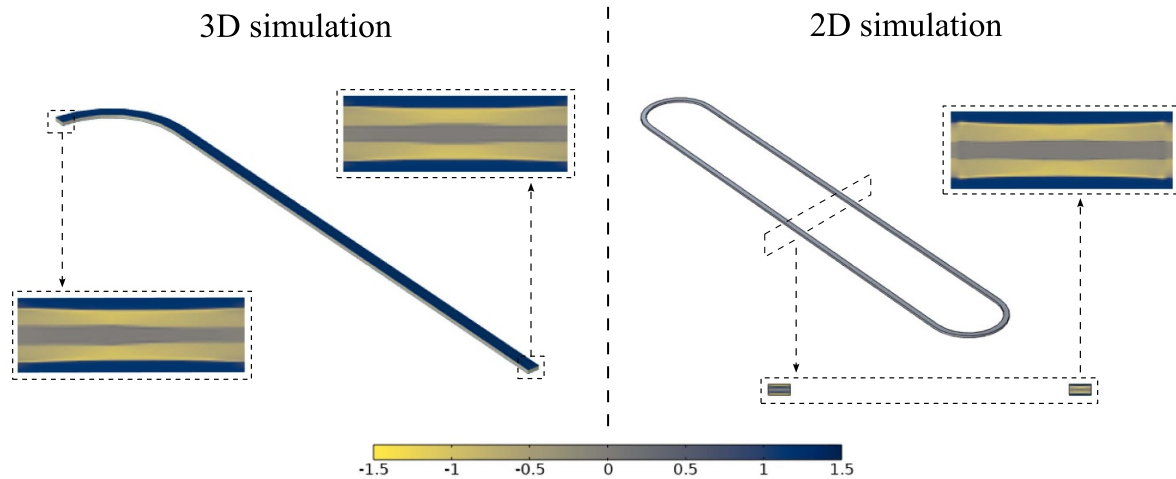


Figure 4. Normalized current density (J/J_c) in coil A for transport current ($f = 18$ Hz and $I_{\text{peak}} = 40$ A – $I_{\text{peak}}/I_c = 85.3\%$) when the current is equal to zero, after the first half period of the sinusoidal cycle. The results of the 3D simulation approach are shown on the left side, with a zoom in the middle of the straight and circular sections. The results of the 2D simulation approach are shown on the right.

is initially developed to analyze the coil. These simulations are based on the homogenization of the T-A formulation in 3D, described in detail in [32]. As it was done in [31], only one-eighth of the coil is modelled by taking advantage of the symmetries.

The left side of figure 4 shows the behaviour of the normalized current penetration (J/J_c) obtained with the 3D simulation. The behaviour of the current penetration is very similar along the length of the coil. Based on these results, it can be assumed that a 2D simulation can also provide a good approximation, even if the geometry is not suitable for a 2D representation. For this reason, a 2D model based on the homogenization of the T-A formulation in 2D is built [33]. This model considers only the middle of the straight section of the coil as an infinite long arrangement. The normalized current penetration behaviour obtained with this 2D simulation is presented on the right side of figure 4. It is in good agreement with the 3D simulation, which confirms the previous hypothesis. A 2D simulation can provide a good approximation in this case.

The AC transport losses estimated for the coil with the 2D and the 3D simulations are summarized in figure 5. The results of the 3D model are presented in blue (triangle symbol) and the 2D model in red (square symbol). The relative error calculated by considering the 3D simulation as the reference is depicted in green (circle symbol). In the 2D simulation case, the results are extended by considering an average turn length to estimate the total losses in the coil. The estimation of the losses done with the 2D and 3D models are in good agreement, with a maximum relative error lower than 7%. The 3D model has 266.663 degrees of freedom (DOF), and the 2D model has 19.656 DOF. This massive reduction in DOF allows a reduction in the computation time from days (in the 3D model case study) to minutes (in the 2D model case study) within reasonable accuracy.

As it was done with the inductance, the critical current (I_c) of the coil is estimated first with simulations based on the methodology presented in [34]. This approach was already

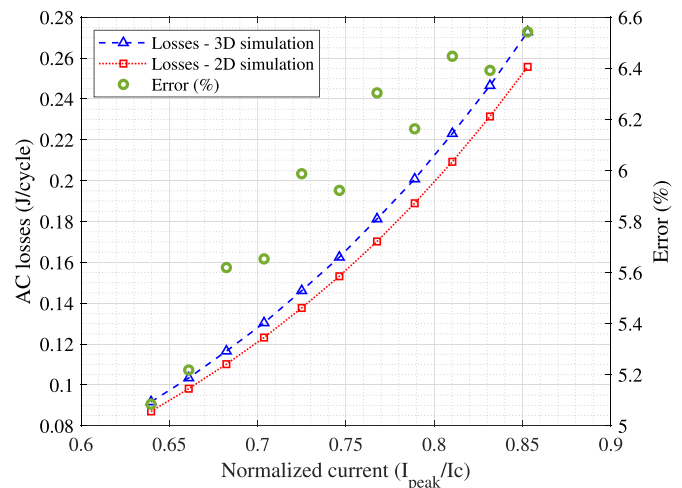


Figure 5. Results of the estimation of AC transport losses in coil A made with 3D and 2D models based on the homogenization of the T-A formulation. The green circles represent the relative error calculated by using the 3D simulation as the reference. The horizontal axis is normalized by considering a critical transport current $I_c = 46.89$ A.

used to estimate the critical current of HTS coils [35–37]. The methodology establishes two criteria to estimate the critical current in the coil, the so-called maximum and the average criteria. The maximum criterion defines I_c as the current that produces a voltage drop per unit length equal to the critical electric field ($E_c = 1 \mu\text{V cm}^{-1}$) in at least one turn of the coil. The average criterion defines I_c as the current that produces an average voltage drop in the coil (all turns) equal to E_c [34]. A 2D model is used to calculate I_c by following a similar approach to [35, 38]. This model considers only the middle of the straight section of the coil. The estimated critical current of the coil is 45.94 A with the maximum criterion and 46.89 A with the average criterion. The measured critical current of the coil with a $1 \mu\text{V cm}^{-1}$ criterion is 44.27 A. This result is

in good agreement with the simulations. It has a deviation of 3.77% and 5.92% with respect to the maximum and average criterion respectively, by considering the measurement result as the reference.

3. Design and construction of the measurement setup

The design of the calorimetric setup to measure AC transport losses is divided into five main parts: cryostat and bubble collector, power supply, current measurement, flow measurement, and data and acquisition system. Figure 6 shows a schematic of the setup with all its components. The coil is located inside a rectangular box that represents the cryostat and bubble collector, and it is energized through an AC voltage source and a current transformer. The current through the coil is measured with a Rogowski coil and the evaporation of the cryogen is directed into a flow sensor. The main variables are collected and recorded with the data acquisition system (indicated with dashed lines) and plotted in real-time on the computer. In this subsection, we will focus on the description, design, and selection of each of these components.

Figure 6 shows also a DC voltage source and a resistance that is used for calibration. This part of the setup will be explained in section 4, which describes the calibration of the setup and the reproducibility of the results.

3.1. Cryostat and bubble collector

One of the main sources of noise that can affect the flow of evaporated nitrogen is the interaction with the environment. Since the coil is at cryogenic temperature, there is a continuous heat transfer from the surroundings into the internal part of the cryostat. This phenomenon causes additional evaporation of the cryogen that can influence the measurements. Moreover, the heat transfer depends on ambient conditions. It changes through the day and between different days and weeks (it can not be fully predicted or controlled). Therefore, the design of the cryostat and bubble collector plays a key role in the accuracy of the measurement setup. For this reason, a box-inside-a-box approach is implemented to minimize the heat transfer and avoid a thick cryostat. During the experiments, the internal box is completely filled and the external box is partially filled with liquid nitrogen. This approach allows redirecting the heat transfer from the surroundings into an intermediate zone (space between external and internal box). Since this intermediate zone operates at cryogenic temperatures, the heat transfer to the internal part of the setup is reduced despite the thickness or material of the cryostat. Therefore, two commercial expanded polypropylene boxes are used for this application.

Figure 7 shows a 3D rendering of the assembly of the setup. The bubble collector has a semi-cylindrical shape that allows gathering the evaporated cryogen. It is raised 5 cm to avoid any additional heat transfer from the bottom of the setup. The bubbles are collected on half of the coil to avoid the

evaporation coming from the connectors and to measure the losses only in the superconducting turns. These parts of the setup were 3D printed by using glass-filled fine polyamide, which withstands thermal stress and provides good sealing.

There are four small slots between the top and bottom parts of the bubble collector that allow the refilling of the cryogen. A basic estimation of the hydrostatic pressure was done and compared with the drop of pressure in the flow meter to ensure a proper flow of the gas. As a result, a minimum level of 25 cm of liquid nitrogen is kept in the inner box during all the measurements.

All the measurements and calibrations presented in this manuscript are done with the cryostat and bubble collector described in figure 7, which includes the box-inside-a-box approach.

3.2. Power supply

The power supply consists of a lock-in amplifier (model 7265 manufactured by AMETEK®) that generates a reference sinusoidal signal (with variable amplitude and frequency) and measures the voltage in a Rogowski coil used to measure the transport current in the superconductive coil. The reference output from the lock-in amplifier is connected with a power amplifier (HERO®—power, model PA2033A) which provides the power to energize the coil. Finally, the output of the power amplifier is connected with the superconducting coil through a current transformer that provides insulation and adjusts the voltage and current capacity of the power supply to the requirements of the coil.

3.3. Current measurement

The current that flows through the HTS coil is measured by using two approaches. The first one is based on a Rogowski coil that works as a current transducer. This coil captures the magnetic field around the cable that feeds the current into the coil. Therefore, the voltage at the terminals of the Rogowski coil is directly related to the current flowing through the cable. This voltage is measured with the lock-in amplifier and it is translated into current in ampere with a previously measured calibration curve. The current is also measured with a commercially available clamp meter (model U1212A manufactured by Agilent), which provides a local visual measurement of the current.

3.4. Flow measurement

The evaporated nitrogen is measured with a flowmeter manufactured by Teledyne Hastings Instruments, which consists of a power supply with a local indication of flow (model ENALL-5KPG) and a transducer (model HS-5KS) calibrated for nitrogen with a measurement range of 5 standard litres per minute (SLPMs) [39]. The power supply also has an analog output of 0 to 5 V DC linearly related to the measured flow (0 to 5 SLPM). This analog output is used by the data and acquisition system to plot and record the measurements.

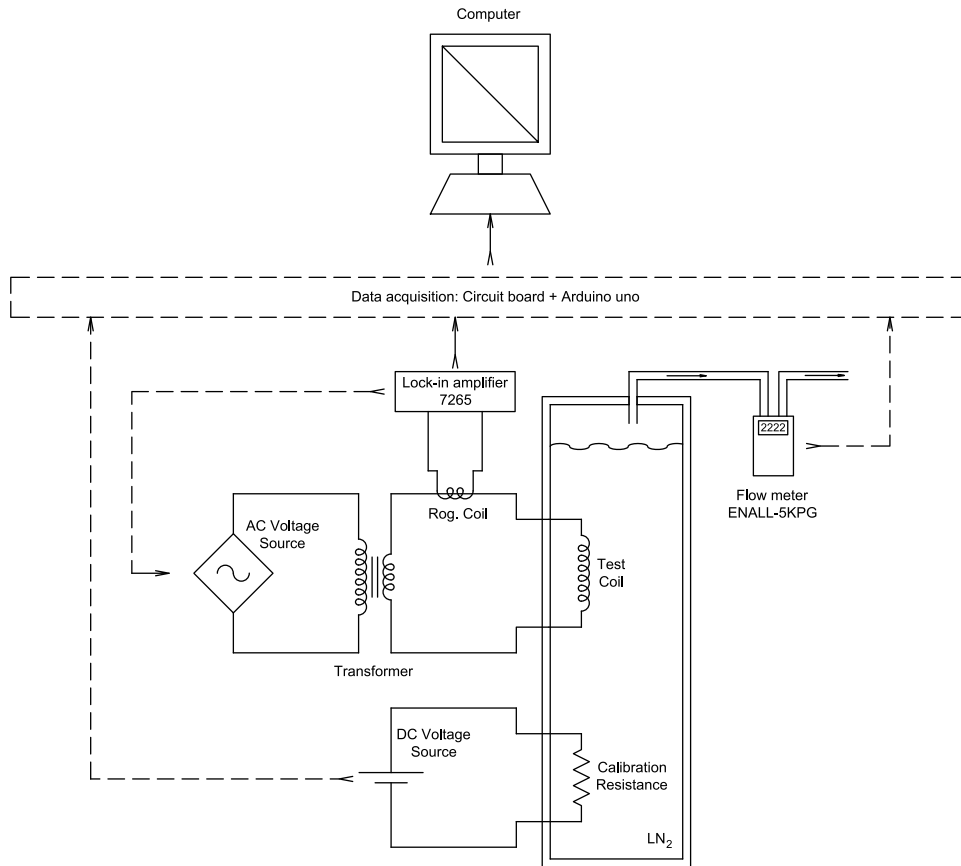


Figure 6. Diagram of the setup to measure AC transport losses in HTS coils through a calorimetric approach.

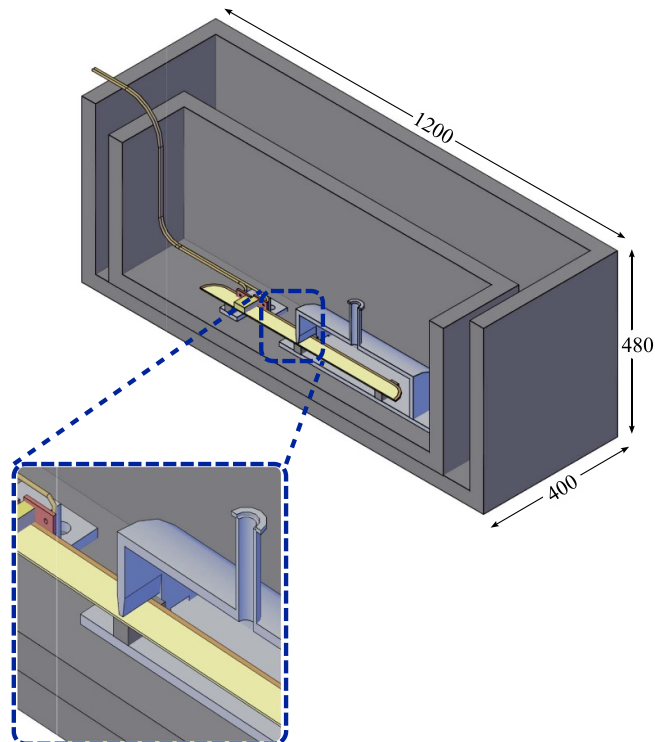


Figure 7. Assembly of the cryostat and bubble collector of the setup to measure AC transport losses in HTS coils through a calorimetric approach. All the dimensions are in millimeters.

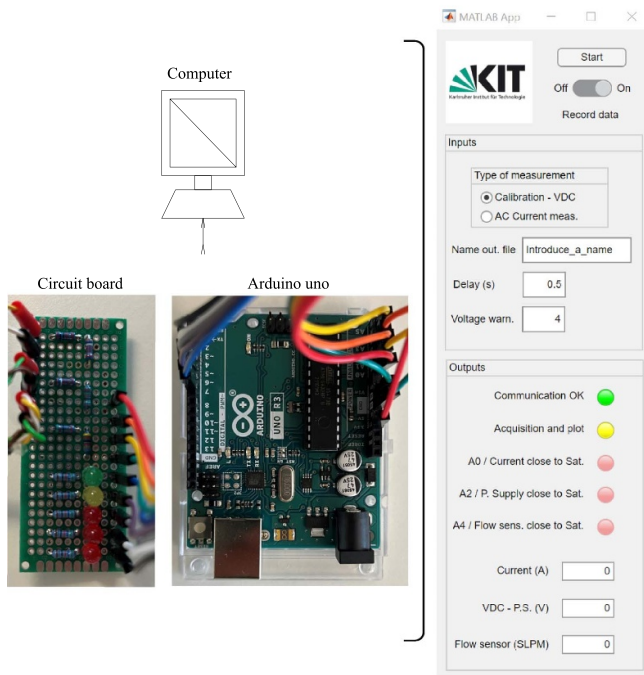


Figure 8. Data acquisition system of the setup to measure AC transport losses.

3.5. Data acquisition system

The main variables are collected in a small circuit board manufactured internally, which consists of a set of voltage dividers used to adapt the range of the voltage to be measured to the maximum analog voltage input of an Arduino Uno. This small board also incorporates one green LED that indicates the system is ON, one yellow LED that indicates the system is recording, and three red LEDs that provide warnings in over-voltage conditions. The board is connected to an Arduino Uno, which communicates with a computer to plot and to record the signals (figure 8).

A graphical user interface (GUI) was created in MATLAB® to plot and record the collected data, as shown on the right side of figure 8. In this GUI, the user can give a name to the output file and select a possible delay between measurements. It also shows the current values of the flow in SLPM, current in ampere, and DC voltage (used for calibrations) together with a visual representation of the LEDs included in the small circuit board. A plot of the recorded values is shown while the program is recording, and when it stops a file (in Microsoft Excel format) is created with all the recorded data.

4. Calibration of the setup and measurements of AC transport losses in the HTS coil

Once the setup is designed and built, the following steps are the calibration and measurements of the AC transport losses. Figure 9 shows the setup layout with a HTS coil inside. The black boxes are the internal and external cryostats, and the white part is the 3D-printed bubble collector. Before measuring the AC transport losses in the coil, it is necessary to build

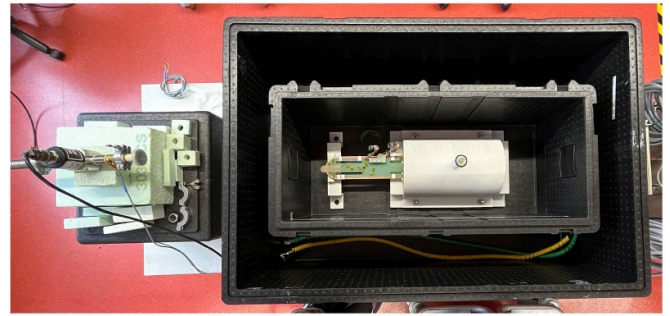


Figure 9. Setup to measure AC transport losses with a HTS racetrack coil inside. From left to right, we have the flow transducer, internal and external cryostat (black boxes), and bubble collector (white 3D printed parts).

the calibration curve that allows translating the evaporated nitrogen (in SLPM) into dissipation (in watt). Moreover, it is important to check the reproducibility of the measurements by repeating and comparing different measurements under different conditions. This verifies the influence of the environment on the measurements and the reliability of the measurement setup. In this subsection, the construction of the calibration curve and the verification of the reproducibility are presented. Since these are the first measurements with the setup, the post-processing procedure and load cycles of the measurements are described.

4.1. Calibration resistor

The calibration curve of the setup is built by producing a controlled dissipation of energy inside the bubble collector. For this reason, an arrangement of three 25 W 39 Ω resistors connected in parallel is used. The resistance of the arrangement is measured previously in cold (covered by liquid nitrogen) and warm (ambient temperature) conditions multiple times with variations lower than 0.3 Ω . This configuration of resistors is energized with a DC power supply (model QL355P manufactured by Aim and Thurlby Thandar Instruments). Since the value of the equivalent resistance is known, the dissipation of energy can be controlled by changing the DC voltage in the power supply.

4.2. Load cycle and post-processing technique

The measurements are structured in load cycles, by following a similar approach to the one introduced in [22]. Each load cycle represents one value of dissipated energy and lasts 60 min. During the first 30 min, the DC voltage (or AC current in the coil) remains constant at a specific value and the evaporation of the cryogen related to the dissipated energy in the resistor (coil) is measured. Then the DC voltage (AC current in the coil) is reduced to zero. During the next 30 min, the background flow is measured. This approach creates a clear distinction between load cycles, allows re-filling of liquid nitrogen during the whole measurement time.

Figure 10 presents the behaviour of the flow of evaporated cryogen in one set of measurements done with the calibration

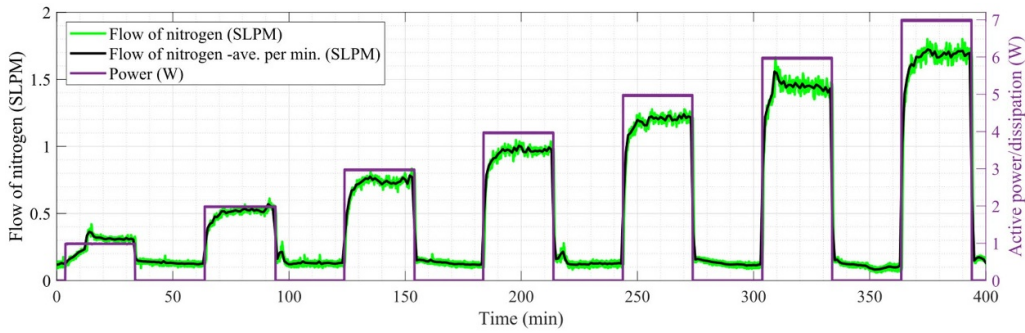


Figure 10. Measurement of the evaporation of nitrogen due to the dissipation of energy in the calibration resistance.

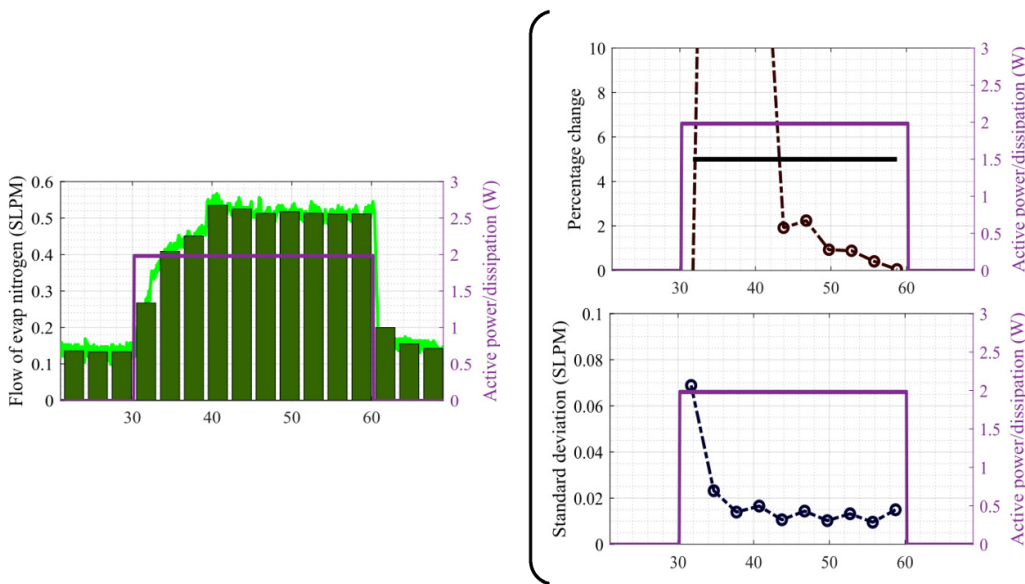


Figure 11. Post-processing of one load cycle of the evaporation of nitrogen due to the dissipation in the calibration resistance.

resistors. The active power (purple line and right axis) in the resistors was changed from 1 W up to 7 W. The flow of evaporated nitrogen (light green and left axis) shows a continuous fluctuation during the whole measurement range. Similar variations were reported in other application that followed the same measurement principle [22, 23]. This behaviour can be related to how the bubbles are created and collected in the measurement chamber. The dark green plot in figure 10 shows the behaviour of the average per minute flow of evaporated cryogen. There is still a significant fluctuation even if we take the average per minute. Therefore, a more complex post-processing technique must be implemented to properly assess the uncertainty of the measurements.

For the post-processing of the data, each 30 min section of the load cycle is subdivided into ten time slots of 3 min each. The average value of the evaporated nitrogen is calculated in each time slot, as shown on the left side of figure 11, where the instantaneous flow is in light green and the average values are in dark green bars. In this plot, we can see a transient behaviour that starts once the arrangement of resistors is energized. The percentage variation of the average flow between time slots is calculated to establish the beginning and end of the transient

behaviour. For this purpose, a 5% criterion is used. If the percentage variation is lower than 5%, we can say that a steady state was reached. If the percentage variation is higher than 5%, we can say that we still have a transient behaviour.

The standard deviation (σ) is also calculated in each time slot to assess the uncertainty in the measurements. As shown in the bottom right corner of figure 11, the standard deviation also exhibits a transient behavior that ends once the percentage variation of the average flow is below 5%. After this point, it only has very small fluctuations. Finally, the measurements can be written as an average value plus and minus two times the standard deviation, which represents an uncertainty range that includes 95.4% of the data in the last time slots if we assume a normal distribution [40].

4.3. Reproducibility

The measurements of evaporated nitrogen related to 1 W and 2 W of dissipation in the calibration resistors were repeated to verify the reproducibility of the results under different ambient conditions and resistors arrangements. Figure 12 shows the arrangements of resistors used to verify the reproducibility.

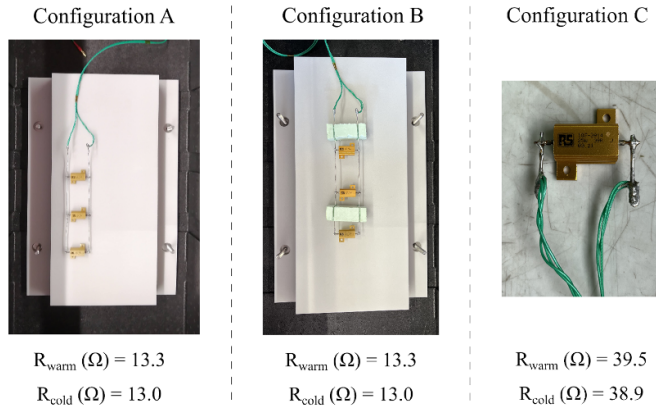


Figure 12. Configuration of resistors used to verify the reproducibility of the measurements.

Table 2. Evaporation of cryogen due to the dissipation of energy in the configurations of resistors used to verify the reproducibility.

Configuration	Power (W)	Average flow (SLPM)	Uncertainty - $2 \cdot \sigma$ (SLPM)
A	1	0.31	0.02
	2	0.51	0.02
B	1	0.32	0.02
	2	0.52	0.02
C	1	0.31	0.02
	2	0.52	0.04

The resistance of each arrangement is measured in cold (covered by liquid nitrogen) and warm (ambient temperature) conditions. For simplicity, the configuration of resistors used in the set of measurements presented in figure 10, is named configuration A. This arrangement is modified by adding two small blocks of styrodur in configuration B. The main objective of this change is to raise the three resistors 1.5 cm to allow liquid nitrogen at the bottom of the arrangement and test a different position of the resistors in the measurement chamber. Finally, configuration C is made with only one single resistor. This allows verifying whether changes in the number of resistors have an impact on the measurements. Each configuration is measured on different weeks. After each measurement, the whole setup is disassembled, dried, cleaned, and re-assembled.

Table 2 presents the results of the measurements of evaporation of cryogen due to the dissipation of energy in the configurations of resistors used to verify the reproducibility. All the measurements are in good agreement with each other. The differences between measurements are small and within the uncertainty range. This confirms the reliability of the measurement setup by reproducing the same results under different ambient conditions, different weeks and different configurations of calibration resistors.

4.4. Calibration curve

After the reproducibility of the measurements is verified, we can proceed and build the calibration curve. For this purpose, the post-processing procedure described previously

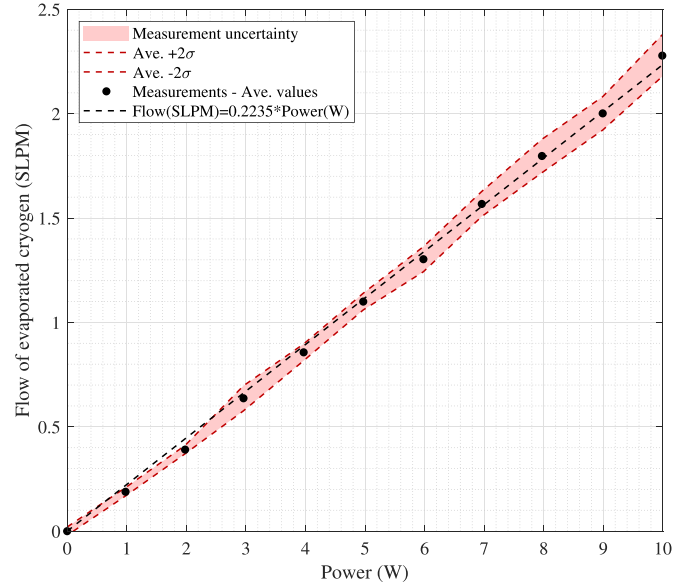


Figure 13. Calibration curve of the setup to measure AC transport losses.

is followed to analyze the data shown in figure 10. The background flow was stable around an average value of 0.12 with an uncertainty of 0.02 SLPM.

Figure 13 presents a plot of the calibration curve once the background flow is subtracted from the measurements. The black dots represent the average values, and the dashed red lines and light red zone represent the uncertainty in the measurements. The dashed black line presents a linear fit to the experimental data with a coefficient of determination of 0.9985. This linear fit provides a practical relation between the dissipated energy in the measurement chamber and the average flow of evaporated nitrogen, which means that 1 W of dissipation inside the measurement chamber produces a flow of 0.2235 SLPM of evaporated nitrogen.

The calibration curve shown in figure 13 is only valid for the range of heat dissipation indicated in this plot and measured in this work. Extrapolation of this data may lead to inaccuracies.

The AC transport loss measurements in the coil are summarized in figure 14, which presents the AC losses as a function of the normalized current (I/I_c). The measurement data is normalized by considering the measured critical current with a $1 \mu\text{V cm}^{-1}$ criterion (44.27 A) and the simulation results are normalized by considering the critical current calculated with the 2D model and average criterion (46.89 A). In this graph, the losses estimated with 3D simulations are presented in blue and the measurements in red. Each average flow measurement (F) is translated into watt by using the following equation:

$$P(\text{W}) = \frac{2}{0.2235 \frac{\text{SLPM}}{\text{W}}} \cdot F(\text{SLPM}). \quad (1)$$

The propagation of the uncertainty (δP) is calculated as described in [40]:

$$\delta P = \frac{d(P)}{dF} \cdot \delta F \quad (2)$$

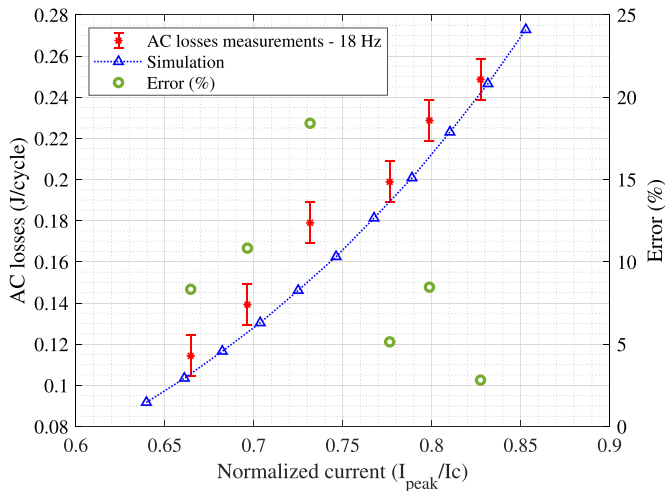


Figure 14. AC transport losses measurements in the coil A, and comparison with simulation results calculated with the homogenization of the T-A formulation in 3D.

$$\delta P = \frac{4}{0.2235 \frac{\text{SLPM}}{\text{W}}} \cdot \sigma(\text{SLPM}). \quad (3)$$

In these equations, δF represents the uncertainty in the flow measurements calculated as two times the standard deviation ($2 \cdot \sigma$).

Figure 14 also shows the relative error in the measurements by considering the 3D simulation results as the reference. The measurements are in good agreement with the simulations with a maximum error lower than 19%.

The differences between measurements and simulations can be related to the considerations and assumptions made in the development of the simulation model and the measurement technique. The modelling approach is based on the homogenization of the T-A formulation, since a detailed representation of the tape can lead to a problem with too many DOF to be solved with the currently commercially available computation power. Therefore, the detailed structure of the tape is not considered [32]. Moreover, the inhomogeneities of the critical current of the tape along the length are neglected. These inhomogeneities are not easy to predict, since they change between different production batches and manufacturers. Furthermore, there is an uncertainty in the measurements related to the variability of the evaporated cryogen. These are some of the main assumptions and considerations. Therefore, minor discrepancies are expected between AC loss measurements and simulation results. These discrepancies are typical in this type of measurement, as shown in [41–44], where similar variations between the estimated and measured AC losses are reported for different approaches. The measurement results agree with the accuracy reported in [11, 19] for similar measurement techniques.

The reproducibility of the results presented in figure 14 is verified by repeating three of the measurements on a different week, after the whole setup is disassembled, dried, cleaned, and re-assembled. The results of this verification are summarized in table 3. The differences between measurements are small and within the uncertainty range. These results confirm

Table 3. Evaporation of the cryogen related to the dissipation of energy in the racetrack coil due to an AC transport current with a frequency of 18 Hz and variable amplitude.

Week	I/I_c	Flow $F(\text{SLPM})$	Uncertainty $\delta P(\text{SLPM})$	AC losses $P(\text{W})$	Uncertainty $\delta P(\text{W})$
A	0.66	0.35	0.02	2.06	0.36
	0.73	0.48	0.02	3.22	0.36
	0.80	0.58	0.02	4.12	0.36
B	0.67	0.37	0.02	2.24	0.36
	0.73	0.48	0.02	3.22	0.36
	0.80	0.60	0.02	4.30	0.36

the reliability of the measurement setup to measure AC transport losses in HTS racetrack coils.

5. Conclusion

In this work, the design, construction, and test of a setup for the calorimetric measurement of AC transport losses were presented. The measurement approach is based on the boil-off method. A bubble collector was designed and 3D printed to guide the evaporation of the cryogen into a flow meter. A box-inside-a-box solution was implemented to minimize the influence of the environment, and a statistical analysis of the results was done. This statistical treatment of the fluctuations in the evaporated cryogen is new for this type of measurement, and it allows expressing the variability in the flow as uncertainty in the measurements.

The reproducibility of the measurements was verified with different arrangements of resistors during the calibration stage. The measurements were in good agreement with a maximum deviation of 0.01 SLPM. Moreover, AC transport losses measurements in the HTS coil were also repeated. The maximum variation was 0.18 W in this case. Each set of measurements was done in a different week after the whole setup was disassembled, dried, cleaned, and re-assembled. The reported deviations are within the uncertainty range of the measurements. The excellent reproducibility of the results under different conditions represents an exceptional outcome in the field of AC loss measurements based on a calorimetric approach (boil-off method) since the strong influence of the environment can cause fluctuations that are not easy to reproduce. These results can be related to the implemented creative solutions, such as the box-inside-a-box approach and the statistical analysis. The first reduces the influence of the environment and the second allows assessing the maximum level of deviation that can be accepted in the measurements to agree that the results are the same. Moreover, the 3D-printed bubble collector solution introduces flexibility in the measurement approach. Therefore, it can be easily extended to more complex geometries and applications.

The construction and characterisation of a HTS racetrack coil were introduced as the first measurement case. The inductance and critical current of the coil were first estimated with finite-element models and compared with measurements. A good agreement between simulations and measurements

was found in both cases, with a maximum deviation of 8.12% in the inductance and 5.92% in the critical current. The coil was modeled by using the homogenization of the T-A formulation in 2D and 3D to estimate AC transport losses. The normalized current penetration and loss estimations were shown and compared between both models, where a maximum relative error lower than 7% was found for the 2D AC loss approximation. Finally, the AC transport losses were measured in the coil and a good agreement with the simulations was found (maximum error lower than 19%). These results confirm the reliability and accuracy of the measurement setup.

Data availability statement

All data that support the findings of this study are included within the article (and any supplementary files).

Acknowledgments

The underlying work of this article was funded by the German Federal Ministry for Economic Affairs and Energy (project name ‘SupraGenSys’, funding reference number 03EE3010C and 03EE3010D). The responsibility for the content of this article lies with the authors and does not necessarily reflect the opinion of the SupraGenSys project consortium.

The authors thank Dustin Kottonau, Fabian Schreiner and Andrej Kudymow for sharing comments regarding AC loss measurement approaches in HTS applications that fed fruitful discussions during the development of this work.

ORCID iDs

Carlos Roberto Vargas-Llanos  <https://orcid.org/0000-0001-7214-3076>

Francesco Grilli  <https://orcid.org/0000-0003-0108-7235>

References

- [1] Kalsi S S 2011 *Applications of High Temperature Superconductors to Electric Power Equipment* (Hoboken, NJ: Wiley)
- [2] Haran K S *et al* 2017 High power density superconducting rotating machines—development status and technology roadmap *Supercond. Sci. Technol.* **30** 123002
- [3] Rong C C and Barnes P N 2017 Developmental challenges of SMES technology for applications *IOP Conf. Ser.: Mater. Sci. Eng.* **279** 012013
- [4] Okakwu I K, Orukpe P E and Ogujor E A 2018 Application of superconducting fault current limiter (SFCL) in power systems: a review *Eur. J. Eng. Res. Sci.* **3** 28–32
- [5] Abrahamsen A, Magnusson N, Jensen B and Runde M 2012 Large superconducting wind turbine generators *Energy Proc.* **24** 60–67
- [6] Kalsi S S 2014 Superconducting wind turbine generator employing MgB₂ windings both on rotor and stator *IEEE Trans. Appl. Supercond.* **24** 5201907
- [7] Sanz S, Arlaban T, Manzanar R, Tropeano M, Funke R, Kováč P, Yang Y, Neumann H and Mondesert B 2014 Superconducting light generator for large offshore wind turbines *J. Phys.: Conf. Ser.* **507** 032040
- [8] Liu D, Polinder H, Abrahamsen A B and Ferreira J A 2015 Comparison of 10 MW superconducting generator topologies for direct-drive wind turbines *2015 IEEE Int. Electric Machines & Drives Conf. (IEMDC)* (Coeur d’Alene, ID: IEEE) pp 174–80
- [9] Winkler T (EcoSwing Consortium) 2019 The EcoSwing project *IOP Conf. Ser.: Mater. Sci. Eng.* **502** 012004
- [10] Wesche R 2015 *Physical Properties of High-Temperature Superconductors* (New York: Wiley)
- [11] Wang Y, Guan X and Dai J 2014 Review of AC loss measuring methods for HTS tape and unit *IEEE Trans. Appl. Supercond.* **24** 9002306
- [12] Zhang H, Wen Z, Grilli F, Gyftakis K and Mueller M 2021 Alternating current loss of superconductors applied to superconducting electrical machines *Energies* **14** 2234
- [13] Frolek L and Šouc J 2011 Measurement of AC transport current loss in different kinds of superconducting tapes and wires in liquid Helium *Supercond. Sci. Technol.* **24** 105016
- [14] Yang Y, Hughes T, Beduz C, Spiller D M, Scurlock R G and Norris W T 1996 The influence of geometry on self-field AC losses of Ag sheathed PbBi2223 tapes *Physica C* **256** 378–86
- [15] Grilli F and Ashworth S P 2007 Measuring transport AC losses in YBCO-coated conductor coils *Supercond. Sci. Technol.* **20** 794–9
- [16] Šouc J, Pardo E, Vojenčiak M and Gömöry F 2008 Theoretical and experimental study of AC loss in high temperature superconductor single pancake coils *Supercond. Sci. Technol.* **22** 015006
- [17] Rabbars J J, 2001 AC loss in superconducting tapes and coils *PhD Dissertation* University of Twente, Twente
- [18] Kim J-H, Kim C H, Iyyani G, Kvitkovic J and Pamidi S 2011 Transport AC loss measurements in superconducting coils *IEEE Trans. Appl. Supercond.* **21** 3269–72
- [19] Okamoto H, Sumiyoshi F, Miyoshi K and Suzuki Y 2006 The Nitrogen boil-off method for measuring AC losses in HTS coils *IEEE Trans. Appl. Supercond.* **16** 105–7
- [20] Eikelboom J 1992 Test results of an apparatus for calorimetric measurement of AC losses in superconductors *IEEE Trans. Magn.* **28** 817–21
- [21] Coletta G, Gherardi L, Gomory F, Cereda E, Ottoboni V, Daney D, Maley M and Zannella S 1999 Application of electrical and calorimetric methods to the AC loss characterization of cable conductors *IEEE Trans. Appl. Supercond.* **9** 1053–6
- [22] Kottonau D 2018 Untersuchung der Machbarkeit eines dreiphasigen CroCo-Leitersystems für supraleitende Energiekabel *Master’s Thesis* University of Duisburg-Essen, Duisburg
- [23] Kottonau D, Wolf M, Fietz W, Stammen J and Hirsch H 2020 Feasibility of ultra-compact HTS CrossConductor based power transmission cables *J. Phys.: Conf. Ser.* **1559** 012084
- [24] Okamoto H, Hayashi H, Sumiyoshi F, Iwakuma M, Izumi T, Yamada Y and Shiohara Y 2007 Nitrogen boil-off method of measuring AC losses in YBCO coils *Physica C* **463–465** 795–7
- [25] Okamoto H *et al* 2008 AC loss properties in YBCO model coils for loss reduction *Physica C* **468** 1731–3
- [26] Kawabata S, Motomura R and Hirayama T 2013 AC loss measurement of high-Tc superconducting coils wound with stacked conductors *IEEE Trans. Appl. Supercond.* **23** 5900904
- [27] Lu J, Bai H, Gavrilin A V, Zhang G, Markiewicz W D and Weijers H W 2015 AC losses of ReBCO pancake coils measured by a calorimetric method *IEEE Trans. Appl. Supercond.* **25** 4701005

- [28] Funakoshi W, Hirayama T and Kawabata S 2022 Measurement of AC loss characteristics of HTS sample coils under the conditions assumed for use in power electronics devices *IEEE Trans. Appl. Supercond.* **32** 5901104
- [29] Molodyk A *et al* 2021 Development and large volume production of extremely high current density $\text{YBa}_2\text{Cu}_3\text{O}_7$ superconducting wires for fusion *Sci. Rep.* **11** 2084
- [30] Vargas-Llanos C R, Lengsfeld S, Noe M, Arndt T and Grilli F 2021 Influence of coil position on AC losses of stator superconducting windings of a synchronous machine for a 10 MW wind turbine *IEEE Trans. Appl. Supercond.* **31** 5206509
- [31] Zermeño V M R and Grilli F 2014 3D modeling and simulation of 2G HTS stacks and coils *Supercond. Sci. Technol.* **27** 044025
- [32] Vargas-Llanos C R, Huber F, Riva N, Zhang M, and Grilli F 2022 3D homogenization of the T-A formulation for the analysis of coils with complex geometries (arXiv:2206.09718 [cond-mat.supr-con])
- [33] Berrospe-Juarez E, Zermeño V M R, Trillaud F and Grilli F 2019 Real-time simulation of large-scale HTS systems: multi-scale and homogeneous models using the T–A formulation *Supercond. Sci. Technol.* **32** 065003
- [34] Zermeño V, Sirois F, Takayasu M, Vojenciak M, Kario A and Grilli F 2015 A self-consistent model for estimating the critical current of superconducting devices *Supercond. Sci. Technol.* **28** 085004
- [35] Liu Y, Ou J, Grilli F, Schreiner F, Zermeño V M R, Zhang M and Noe M 2018 Comparison of 2D simulation models to estimate the critical current of a coated superconducting coil *Supercond. Sci. Technol.* **32** 014001
- [36] Liu D, Xia J, Yong H and Zhou Y 2016 Estimation of critical current distribution in $\text{Bi}_2\text{Sr}_2\text{CaCu}_2\text{O}_x$ cables and coils using a self-consistent model *Supercond. Sci. Technol.* **29** 065020
- [37] Gong T, Ma G, Xiao L, Li J, Zhou P, Xie P and Liu B 2022 Critical current estimation of HTS coil considering the tape inhomogeneity and different criteria *IEEE Trans. Appl. Supercond.* **32** 4601505
- [38] Liu Y 2018 Design of a superconducting DC wind generator *PhD Dissertation* Karlsruhe Institute of Technology, Karlsruhe (available at: <https://publikationen.bibliothek.kit.edu/1000083023>)
- [39] NALL mass flowmeters Product manual 111-122010, December 2022, revision G. (Hampton, Virginia: Teledyne Hastings Instruments) (available at: www.teledyne-hi.com/products/Thermal_Mass_Flow_Products/Pages/NALL-Series.aspx)
- [40] Taylor J R 1982 *An Introduction to Error Analysis: The Study of Uncertainties in Physical Measurements* 1st edn (Mill Valley, CA: University Science Books)
- [41] Pardo E, Šouc J and Kováč J 2012 AC loss in ReBCO pancake coils and stacks of them: modelling and measurement *Supercond. Sci. Technol.* **25** 035003
- [42] Ainslie M 2012 Transport AC loss in high temperature superconducting coils *PhD Dissertation* University of Cambridge, Cambridge (available at: www.repository.cam.ac.uk/handle/1810/244077)
- [43] Ainslie M D, Yuan W, Hong Z, Pei R, Flack T J and Coombs T A 2011 Modeling and electrical measurement of transport AC loss in HTS-based superconducting coils for electric machines *IEEE Trans. Appl. Supercond.* **21** 3265–8
- [44] Gömöry F, Šouc J, Pardo E, Seiler E, Soloviev M, Frolek L, Skarba M, Konopka P, Pekarčíková M and Janovec J 2013 AC loss in pancake coil made from 12 mm wide REBCO tape *IEEE Trans. Appl. Supercond.* **23** 5900406